



Cooperative plasmon enhanced organic solar cells with thermal coevaporated Au and Ag nanoparticles



Yuan Gao ^{a,b}, Fangming Jin ^a, Zisheng Su ^{a,*}, Haifeng Zhao ^a, Yongshi Luo ^a, Bei Chu ^{a,**}, Wenlian Li ^a

^a State Key Laboratory of Luminescence and Applications, Changchun Institute of Optics, Fine Mechanics, and Physics, Chinese Academy of Sciences, Changchun, 130033, People's Republic of China

^b University of Chinese Academy of Sciences, Beijing, 100039, People's Republic of China

ARTICLE INFO

Article history:

Received 13 April 2017

Received in revised form

16 May 2017

Accepted 1 June 2017

Available online 10 June 2017

Keywords:

Organic solar cell

Small molecule

Localized surface plasmon resonance

MoO₃ buffer layer

Au:Ag nanoparticle

ABSTRACT

Cooperative plasmon enhanced small molecule organic solar cells are demonstrated based on thermal coevaporated Au and Ag nanoparticles (NPs). The optimized device with an appropriate molar ratio of Au:Ag NPs shows a power conversion efficiency of 3.32%, which is 22.5% higher than that of the reference device without any NPs. The improvement is mainly contributed to the increased short-circuit current which resulted from the enhanced light harvesting due to localized surface plasmon resonance of Au:Ag NPs and the increased conductivity of the device. Besides, factors that determining the performance of the Au:Ag NPs cooperative plasmon enhance organic solar cells are investigated, and it finds that the thickness of MoO₃ buffer layer plays a crucial role. Owing to the different diameter of the thermal evaporated Au and Ag NPs, a suitable MoO₃ buffer layer is required to afford a large electromagnetic enhancement and to avoid significant exciton quenching by the NPs.

© 2017 Elsevier B.V. All rights reserved.

1. Introduction

Organic solar cells (OSCs) have attracted a lot of attention due to their low weight, low cost, and flexibility. Recently, the performance of organic solar cells (OSCs) increased very quickly and the power conversion efficiency (PCE) has been reported over 10% [1–10]. However, their PCE is still lower than their inorganic counterparts, and much effort should be applied for further improvement. The PCE of OSCs is determined by their absorption efficiency, exciton dissociation efficiency, and charge carrier collection efficiency. Although organic materials have a large extinction coefficient in visible to near-infrared wavelengths, they cannot absorb all the solar irradiation in these regions. On the other hand, the organic materials usually have low carrier mobility and short exciton diffusion length. A balance between the need of thick active layer to ensure sufficient photon absorption and maintaining thin film due to the relatively low carrier mobility and short exciton diffusion length of organic materials is the main challenge for

enhancing the efficiency of an OSC [11,12]. Thus various light trapping approaches by increasing the absorption of the active layer to increase their efficiency have been explored to solve this issue [13–23]. Among them, incorporating metal nanoparticles (NPs) that support localized surface plasmon resonance (LSPR) into OSCs has been demonstrated as an effective approach to enhance light absorption without increasing the physical thickness of the active layer [24–26]. Besides, the incorporated metal NPs also results in increased conductivity of the devices, which improves their charge carrier collection efficiency.

Plasmon of Au and Ag NPs have been investigated at a large extent in OSCs due to their relative strong scattering efficiency and broad LSPR absorption band in visible range [27–30]. The plasmon effect is controlled by the particle size, shape, spacing, dielectric properties, and dielectric environment, which influence the LSPR peak. Compared with Ag NPs, the higher permittivity of Au NPs leads to longer LSPR wavelength given that they have the same sharp and size. It has been reported that the absorption enhancement ratio is consistent with the LSPR spectrum of the metal NPs [30–34]. To support a large amount of total absorption enhancement, a broad LSPR spectrum is required. Several metal nanostructures have been adopted to meet such a conception, such as the same metal NPs with different sizes [16,35–37], metal

* Corresponding author.

** Corresponding author.

E-mail addresses: suzs@ciomp.ac.cn (Z. Su), chub@ciomp.ac.cn (B. Chu).

nanorods [38–40], and composite NPs with different metals [31,33,41]. Among these methods, mixing of the Au and Ag NPs has gained more attention in the OSCs [30,31,42,43]. In such a strategy, the LSPR spectrum can be tuned easily to the desired spectral range by varying the molar ratio of the Au and Ag NPs. Therefore, the use of Au and Ag NPs mixture in OSCs shows great potential for effective and tunable light trapping, and it has gain more attention in OSCs.

The methods for fabrication of metal NPs can be simply divided into two types, e.g., chemical synthesis and physical deposition [24–26,44–49]. The chemical synthesis methods are easy to prepare metal NPs with monodispersion size. On contrast, the physical deposition methods usually form metal NPs with a wide size distribution, but they can avoid the introduction of organic ligands and other additives. From these points of view, physical deposition methods are more favorable for application in the plasmon enhanced OSCs, especially for small molecule ones. Thermal evaporation is one of the physical deposition methods with the advantages of low cost and simple process. Thermal evaporated Au or Ag NPs have been widely used in plasmon enhanced OSCs [24–26]. Recently, thermal coevaporated Au:Ag composite NPs have been applied in a polymer OSC, and improved PCE has been demonstrated [30,50]. However, there is no report on plasmon enhanced small molecule OSC with thermal coevaporated Au:Ag composite NPs. Moreover, the factors that limiting the performance of the device have not been well exploited. In this work, surface plasmon enhanced 1,1-bis-(4-bis(4-methyl-phenyl)-amino-phenyl)-cyclohexane (DBP)/C₇₀ planar heterojunction small molecule OSCs have been demonstrated based on thermal coevaporated Au:Ag composite NPs. The molar ratio of Au:Ag NPs can be easily tuned by controlling the evaporation rate of the Au and Ag individually. The optimized device with an appropriate molar ratio shows a PCE of 3.32%, which is significantly improved compared with the reference device. More importantly, the factors that determining the performance of these cooperative plasmon enhanced OSCs are discussed.

2. Experimental methods

The organic materials used for the OSCs were procured commercially and were used without further sublimation. Devices were fabricated on patterned indium tin oxide (ITO)-coated glass substrates with a sheet resistance of 15 Ω/sq. Prior to deposition, the ITO substrates were cleaned in a series of solvents such as acetone, deionized water, and isopropyl alcohol, and then treated by ultraviolet-ozone in a chamber for 15 min. All the layers, including Au and Ag NPs, were deposited onto the substrates in sequence via thermal evaporation in the vacuum chamber at a pressure of 4×10^{-4} Pa without a vacuum breaking. Deposition rates were monitored with quartz oscillating crystals and controlled to be 1 Å/s for the metal NPs layers, 0.5 Å/s for MoO₃ and the organic layers, and 5 Å/s for Al cathode. The area of the devices patterned by the shadow mask was 0.1 cm². Current density-voltage (J-V) characteristics of the devices were measured with a Keithley 2400 sourcemeter under an AM 1.5G illumination (Newport 94023A) with a calibrated intensity of 100 mW/cm². The incident photon to current conversion efficiency (IPCE) spectra was performed with a Stanford SR803 lock-in amplifier under monochromatic illumination at a chopping frequency of 130 Hz by a Stanford SR540 chopper. Scanning electron microscopy (SEM) images were measured on a Hitachi S4800. Absorption spectra of the organic films on ITO-coated glass substrates were recorded with a Shimadzu UV-3101PC spectrophotometer. Steady-state photoluminescent (PL) spectra were measured with a Hitachi F7000 fluorescence spectrophotometer. All the measurements were

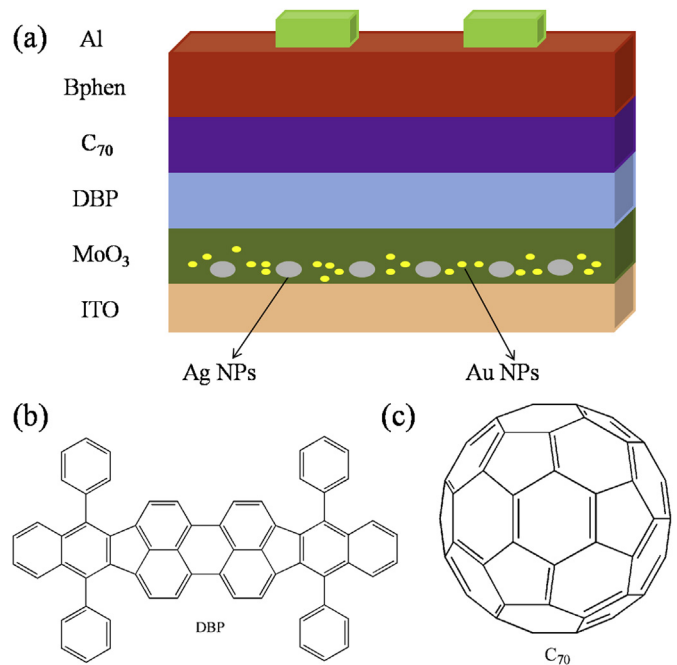


Fig. 1. (a) Device structure of the plasmonic OSCs, and the molecular chemical structures of (b) DBP and (c) C₇₀.

carried out at room temperature under ambient conditions.

3. Results and discussion

A series of devices with the structure of ITO/Au: Ag (x:y) (0.75 nm)/MoO₃/DBP (13 nm)/C₇₀ (45 nm)/4,7-diphenyl-1,10-phenanthroline (Bphen) (8 nm)/Al (100 nm) were constructed, here x:y represented different molar ratio of the Au and Ag NPs, and it differs from 0:1, 2:3, 3:1, and 5:1 to 1:0. For reference, OSCs without any metal NPs were also fabricated. The device structure and molecular structures of DBP and C₇₀ are illustrated in Fig. 1. The thickness of the MoO₃ anode buffer layer plays an important role in determining the performance of the OSCs. Fig. S1–S6 in the Supporting Information describe the J–V curves of the OSCs with different thickness of MoO₃, and the data extracted from these curves are listed in Tables S1–S6 in the Supporting Information, respectively. The optimized thickness of MoO₃ for the reference

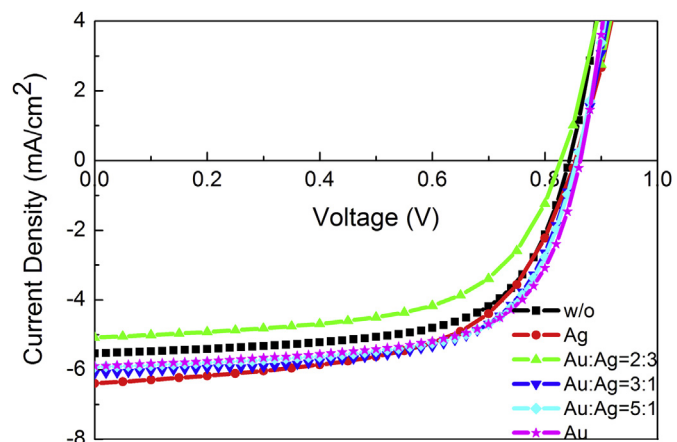


Fig. 2. J–V curves of the optimized devices with different molar ratio of Au:Ag NPs.

Table 1

Photovoltaic parameters of the optimized devices with different molar ratio of Au:Ag NPs.

Au:Ag	MoO ₃ thickness (nm)	Jsc (mA/cm ²)	Voc (V)	FF	PCE (%)	Jsc calculated from IPCE
w/o	2.5 nm	5.53 ± 0.10	0.84 ± 0.01	0.64 ± 0.01	2.98 ± 0.02	5.44
0:1	5 nm	6.39 ± 0.04	0.85 ± 0.01	0.58 ± 0.01	3.19 ± 0.03	6.05
2:3	4 nm	5.09 ± 0.20	0.83 ± 0.01	0.60 ± 0.01	2.53 ± 0.10	5.00
3:1	4 nm	6.11 ± 0.11	0.86 ± 0.01	0.63 ± 0.01	3.32 ± 0.06	5.94
5:1	4 nm	5.92 ± 0.06	0.86 ± 0.01	0.65 ± 0.01	3.30 ± 0.02	5.77
1:0	4 nm	5.89 ± 0.09	0.86 ± 0.01	0.65 ± 0.01	3.29 ± 0.06	5.69

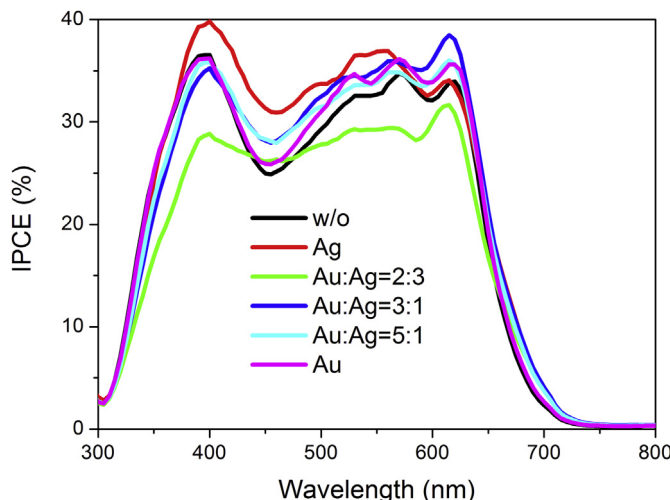


Fig. 3. IPCE spectra of the optimized devices with different molar ratio of Au:Ag NPs.

device is 2.5 nm, while it is 5 nm for 0:1 Au:Ag NPs based device and 4 nm for the other devices.

Fig. 2 displays the J-V curves of the devices with optimized thickness of MoO₃ layers. Each curve is averaged over four devices with the same configuration. The detailed photovoltaic parameters and standard deviations are summarized in Table 1. The reference device without metal NPs layer shows a short-circuit current (Jsc), open-circuit voltage (Voc), fill factor (FF) of 5.53 mA/cm², 0.84 V, 0.64, corresponding to a PCE of 2.98%. The Voc of the devices with metal NPs is comparable to that of the reference device. However, the Jsc and FF exhibit dramatically difference. Among these devices, the device with only Ag NPs has the highest Jsc of 6.39 mA/cm². However, it presents a lowest FF of 0.58. As a result, it shows a PCE of 3.19%. In contrast, the device with only Au NPs has the highest FF

of 0.65 but a low Jsc of 5.89 mA/cm², corresponding to a PCE of 3.29%. Meanwhile, the devices with Au:Ag mixed NPs exhibit moderate Jsc and FF, and the device with a Au:Ag molar ratio of 3:1 has the highest performance. This device shows a Jsc, Voc, FF, and PCE of 6.11 mA/cm², 0.86 V, 0.63, and 3.32%, respectively. This PCE is the highest one among all these devices. Compared with the optimized reference device, the PCE is enhanced by about 11.4%, and such an enhancement is primarily attributed to the improvement of Jsc. Keeping in mind that the reference device with a MoO₃ layer of 4 nm only has a PCE of 2.71% (Fig. S1 and Table S1). This indicates that a 22.5% increase of PCE is obtained if the similar MoO₃ thickness were used.

The enhancement of Jsc is further verified by comparing their IPCE spectra, as shown in Fig. 3. The shape of the IPCE curve is highly dependent on the absorption curve of the active layer. All the devices with metal NPs show increased response in the visible region from 400 to 650 nm except the device with 2:3 Au:Ag NPs. This trend is consistent to the Jsc found in J-V curves. The integrated Jsc values from the IPCE spectra of six devices are 5.44, 6.05, 5.00, 5.94, 5.77 and 5.69 mA/cm², respectively, which are listed in Table 1. These calculated Jsc from this EQE spectrum are a little lower than that obtained from the J-V curve but still within the range of allowable error, indicating good accuracy of our J-V measurement.

To further understand the mechanisms, SEM images of the metal NPs on Si substrates are investigated, as shown in Fig. 4. It can be found that the NPs in bare Au layer are dense with a small average diameter of about 5 nm. In contrast, the NPs in bare Ag layer are sparse with a large average diameter of about 15 nm. However, the Au:Ag mixed layer (3:1) displays a different morphology where both small and large NPs are found. Comparing these three SEM images, we believe that the small NPs are Au NPs, while the large ones are Ag NPs. This finding suggests that the coevaporation of the two metals cannot alter the growth model of them. The large size distribution of the metal NPs is important for surface plasmon enhanced OSCs as they can trigger LSPR over a

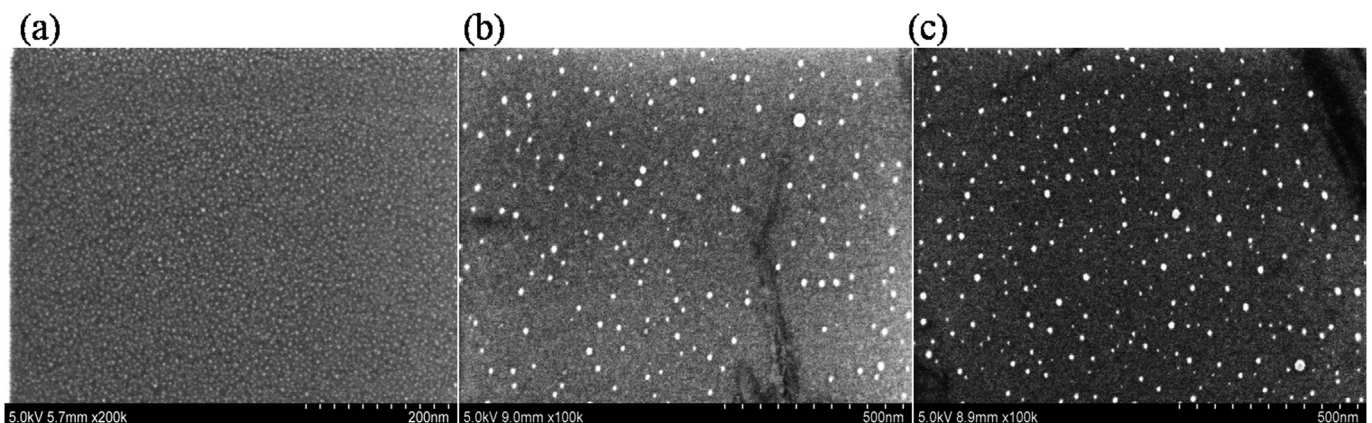


Fig. 4. SEM images of the (a) Au, (b) Ag, and (c) Au:Ag (3:1) NPs on Si wafers.

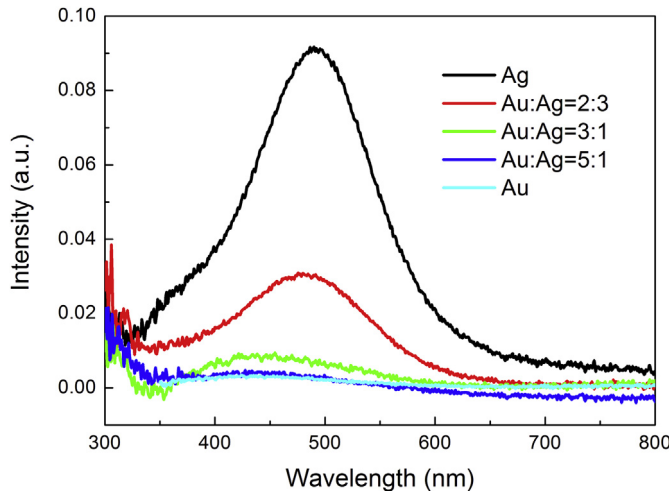


Fig. 5. Absorption spectra of the Au:Ag NPs layers with the different ratio on ITO glass substrates.

wider wavelength range.

The absorption spectra for the metal NPs on ITO-coated glass substrate are also measured, and the corresponding results are shown in Fig. 5. The pure Au NPs show a characteristic peak at about 424 nm, while the pure Ag NPs show a characteristic peak at about 490 nm. The short LSPR peak wavelength of Au NPs is attributed to their small size. It is also noted that the LSPR peak wavelength of Ag NPs is longer than our previous reported ones [24], this should be attributed to the larger size of Ag NPs prepared in this work. Tunable LSPR are observed by adjusting the ratio of Au and Ag NPs. The LSPR absorption peak are 480, 454, and 433 nm for Au:Ag NPs with mixture ratio of 2:3, 3:1, and 5:1, respectively. The LSPR peaks exhibit linear blueshift with the increase of the Au content due to the shorter LSPR peak wavelength of Au NPs.

To better illustrate the contribution of the surface plasmon supported by the metal NPs on the enhancement of J_{sc} , we also investigated the absorption spectra of the DBP/C₇₀ organic films on ITO/NPs/MoO₃, as shown in Fig. 6. During each measurement, the same structure of ITO/NPs/MoO₃ to the sample was used as the reference to exclude the contribution of its absorption to the increase of the absorption of the organic layers. It can be found that

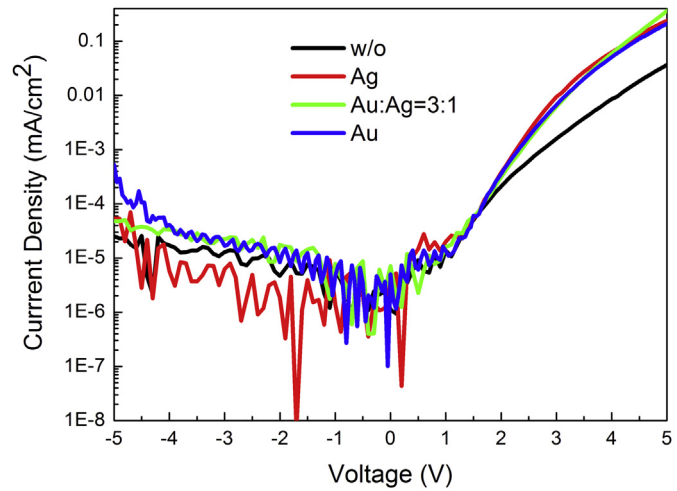


Fig. 7. J-V curves of the hole-only devices ITO/MoO₃/DBP/TAPC/Al with different metal NPs layers.

all the films with metal NPs show an enhanced absorption in the range from 350 to 550 nm. These wavelengths are consistent with the LSPR wavelengths of the NPs, which indicates that the increased absorption of the organic layers is attributed to the electromagnetic enhancement that triggered by the surface plasmon of the metal NPs.

Hole only devices with the structure of ITO/NPs/MoO₃ (the optimized thickness)/DBP (60 nm)/1,1-bis-(4-methyl-phenyl)-amino-phenyl)-cyclohexane (TAPC) (20 nm)/Al (100 nm) have also been fabricated. The dark currents of these devices are drawn in Fig. 7. It can be found that the current densities in positive voltage region of all the devices with metal NPs are almost the same, which are significant higher than that of reference device. This indicates that the conductivity of the devices is increased by incorporation of metal NPs, which is similar to the reported works with the same configurations [24,25].

According to the results found above, it can be concluded that the improved performance of the OSCs with metal NPs is attributed to the increased light harvesting due to LSPR of Au:Ag NPs and the increased conductivity of the device. Thus it is expected that the Au:Ag composite NPs layer which has a broad LSPR absorption will present a high J_{sc} . However, among the devices fabricated here, the device with pure Ag NPs shows the highest J_{sc} , as shown in Fig. 2 and Table 1. From Fig. 5, it can be found that the pure Ag NPs has a highest intensity of LSPR absorption band, which is attributed to the large diameter of the Ag NPs (Fig. 4) [38]. This suggests that the intensity of the LSPR of the metal NPs plays an important role in determining the J_{sc} of the surface plasmon enhanced OSCs. Although the device based on pure Ag NPs has the highest J_{sc} , its lower FF limited its PCE of only 3.19%. The lower FF is attributed to the optimized thicker MoO₃ layer of about 5 nm, which increases the series resistance of the device. On the other hand, Au:Ag (3:1) composite NPs has a broader LSPR band compared with pure Au NPs. However, the device based on this Au:Ag NPs reveals only a slightly higher J_{sc} and PCE. It has been suggested that in the surface plasmon enhanced OSCs, a thick MoO₃ layer is required to fully cover the metal NPs to eliminate exciton quenching of organic layer by the metal NPs and a thin one to support sufficient electromagnetic enhancement in organic layer due to the evanescent wave nature of the surface plasmon. Due to the different diameter of the fabricated Au and Ag NPs, the optimized thickness of MoO₃ layer of the two pure metal NPs based devices is 4 and 5 nm, respectively. The optimized thickness of MoO₃ layer of Au:Ag (3:1) NPs based

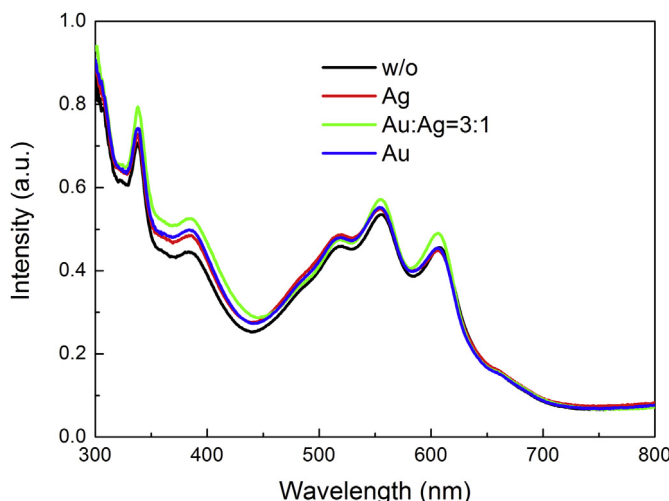


Fig. 6. Absorption spectra of the ITO/NPs/DBP/C₇₀ films with different Au:Ag NPs.

device is only 4 nm. This suggests that some of the Ag NPs may not be fully covered by the MoO₃ layer and hence quench the excitons of DBP. As a result, a moderate J_{sc} is found for this device. This indicates that the advantages of the mixed metal NPs are not fully utilized. To obtain a higher increase of J_{sc} of the surface plasmon enhanced OSCs, composite metal NPs with comparable diameter is required. However, in our experiments, we cannot obtain large size Au NPs with a simple thermal evaporation method even the deposition rate was increased to 3 Å/s. It has been reported that post-thermal annealing can increase the size of the deposited metal NPs [30,51–54]. In such a case, more homogeneous composite metal NPs can be obtained. This work is undergoing in our group and much higher efficiency surface plasmon enhanced OSCs can be expected.

4. Conclusion

In summary, improved performance of DBP/C₇₀ based planer heterojunction OSCs are demonstrated by incorporating the Au:Ag composite NPs. The improvement is attributed to the increased light harvesting due to LSPR of Au:Ag NPs and the increased conductivity of the device. The optimized device shows a peak PCE of 3.32%, which is 22.5% higher than the reference device without metal NPs. However, this PCE is only slightly higher than the devices with pure metal NPs. This is attributed to the quite different size of Au and Ag NPs, and the thickness of MoO₃ layer cannot be simultaneously optimized for these two types metal NPs. This work provides a strategy to obtain high efficiency cooperative plasmon enhanced OSCs based on mixed metal NPs, and this strategy may also be applicable for other types solar cells.

Acknowledgements

This work was supported by the National Natural Science Foundation of China (61376062, 11004187, 61575192, and 61376022) and the Science and Technology Development Plan of Jilin Province (20140201094JC).

Appendix A. Supplementary data

Supplementary data related to this article can be found at <http://dx.doi.org/10.1016/j.orgel.2017.06.003>.

References

- [1] T. Liu, Y. Guo, Y. Yi, L. Huo, X. Xue, X. Sun, H. Fu, W. Xiong, D. Meng, Z. Wang, F. Liu, T.P. Russell, Y. Sun, Ternary organic solar cells based on two compatible nonfullerene acceptors with power conversion efficiency >10%, *Adv. Mater.* 28 (2016) 10008–10015.
- [2] Q. Zhang, X. Wan, F. Liu, B. Kan, M. Li, H. Feng, H. Zhang, T.P. Russell, Y. Chen, Evaluation of small molecules as front cell donor materials for high-efficiency tandem solar cells, *Adv. Mater.* 28 (2016) 7008–7012.
- [3] M. Li, K. Gao, X. Wan, Q. Zhang, B. Kan, R. Xia, F. Liu, X. Yang, H. Feng, W. Ni, Y. Wang, J. Peng, H. Zhang, Z. Liang, H.-L. Yip, X. Peng, Y. Cao, Y. Chen, Solution-processed organic tandem solar cells with power conversion efficiencies >12%, *Nat. Photonics* 11 (2017) 85–90.
- [4] J. Lee, D.H. Sin, B. Moon, J. Shin, H.G. Kim, M. Kim, K. Cho, Highly crystalline low-bandgap polymer nanowires towards high-performance thick-film organic solar cells exceeding 10% power conversion efficiency, *Energy Environ. Sci.* 10 (2017) 247–257.
- [5] D. Baran, T. Kirchartz, S. Wheeler, S. Dimitrov, M. Abdelsamie, J. Gorman, R.S. Ashraf, S. Holliday, A. Wadsworth, N. Gasparini, P. Kaienburg, H. Yan, A. Amassian, C.J. Brabec, J.R. Durrant, I. McCulloch, Reduced voltage losses yield 10% efficient fullerene free organic solar cells with >1 V open circuit voltages, *Energy Environ. Sci.* 9 (2016) 3783–3793.
- [6] S.D. Collins, N.A. Ran, M.C. Heiber, T.-Q. Nguyen, Small is powerful: recent progress in solution-processed small molecule solar cells, *Adv. Energy Mater.* (2017), <http://dx.doi.org/10.1002/aenm.201602242>.
- [7] Y. Liu, C.C. Chen, Z. Hong, J. Gao, Y.M. Yang, H. Zhou, L. Dou, G. Li, Y. Yang, Solution-processed small-molecule solar cells: breaking the 10% power conversion efficiency, *Sci. Rep.* 3 (2013) 3356.
- [8] B. Kan, M. Li, Q. Zhang, F. Liu, X. Wan, Y. Wang, W. Ni, G. Long, X. Yang, H. Feng, Y. Zuo, M. Zhang, F. Huang, Y. Cao, T.P. Russell, Y. Chen, A series of simple oligomer-like small molecules based on oligothiophenes for solution-processed solar cells with high efficiency, *J. Am. Chem. Soc.* 137 (2015) 3886–3893.
- [9] Y. Lin, F. Zhao, Y. Wu, K. Chen, Y. Xia, G. Li, S.K. Prasad, J. Zhu, L. Huo, H. Bin, Z.G. Zhang, X. Guo, M. Zhang, Y. Sun, F. Gao, Z. Wei, W. Ma, C. Wang, J. Hodgkiss, Z. Bo, O. Inganäs, Y. Li, X. Zhan, Mapping polymer donors toward high-efficiency fullerene free organic solar cells, *Adv. Mater.* 29 (2017) 1604155.
- [10] H. Li, D. He, P. Mao, Y. Wei, L. Ding, J. Wang, Additive-free organic solar cells with power conversion efficiency over 10%, *Adv. Energy Mater.* (2017) <http://dx.doi.org/10.1002/aenm.201602663>.
- [11] Z. Yuan, Y. Yang, Z. Wu, S. Bai, W. Xu, T. Song, X. Gao, F. Gao, B. Sun, Approximately 800-nm-thick pinhole-free perovskite films via facile solvent retarding process for efficient planar solar cells, *ACS Appl. Mater. Interfaces* 8 (2016) 34446–34454.
- [12] S.R. Gollu, R. Sharma, G. Srinivas, S. Kundu, D. Gupta, Incorporation of silver and gold nanostructures for performance improvement in P3HT: PCBM inverted solar cell with rGO/ZnO nanocomposite as an electron transport layer, *Org. Electron.* 29 (2016) 79–87.
- [13] C. Fei Guo, T. Sun, F. Cao, Q. Liu, Z. Ren, Metallic nanostructures for light trapping in energy-harvesting devices, *Light Sci. Appl.* 3 (2014) e161.
- [14] S. Pillai, K.R. Catchpole, T. Trupke, M.A. Green, Surface plasmon enhanced silicon solar cells, *J. Appl. Phys.* 101 (2007) 093105.
- [15] Y. Jin, J. Feng, M. Xu, X.-L. Zhang, L. Wang, Q.-D. Chen, H.-Y. Wang, H.-B. Sun, Matching photocurrents of sub-cells in double-junction organic solar cells via coupling between surface plasmon polaritons and microcavity modes, *Adv. Opt. Mater.* 1 (2013) 809–813.
- [16] H.A. Atwater, A. Polman, Plasmonics for improved photovoltaic devices, *Nat. Mater.* 9 (2010) 865.
- [17] F.J. Beck, A. Polman, K.R. Catchpole, Tunable light trapping for solar cells using localized surface plasmons, *J. Appl. Phys.* 105 (2009) 114310.
- [18] F.J. Beck, K. Catchpole, Red-shifting the surface plasmon resonance of silver nanoparticles for light trapping in solar cells, *MRS Proc.* 1101 (2008), 1101-KK03-04.
- [19] X. Chen, B. Jia, Y. Zhang, M. Gu, Exceeding the limit of plasmonic light trapping in textured screen-printed solar cells using Al nanoparticles and wrinkle-like graphene sheets, *Light Sci. Appl.* 2 (2013) e92.
- [20] Q.D. Ou, Y.Q. Li, J.X. Tang, Light manipulation in organic photovoltaics, *Adv. Sci.* 3 (2016) 1600123.
- [21] J.D. Chen, C. Cui, Y.Q. Li, L. Zhou, Q.D. Ou, C. Li, Y. Li, J.X. Tang, Single-junction polymer solar cells exceeding 10% power conversion efficiency, *Adv. Mater.* 27 (2015) 1035–1041.
- [22] B. Paci, G. Kakavelakis, A. Generosi, J. Wright, C. Ferrero, E. Stratikis, E. Kymakis, Improving stability of organic devices: a time/space resolved structural monitoring approach applied to plasmonic photovoltaics, *Sol. Energy Mater. Sol. Cells* 159 (2017) 617–624.
- [23] Q.-D. Ou, H.-J. Xie, J.-D. Chen, L. Zhou, Y.-Q. Li, J.-X. Tang, Enhanced light harvesting in flexible polymer solar cells: synergistic simulation of a plasmonic meta-mirror and a transparent silver mesowire electrode, *J. Mater. Chem. A* 4 (2016) 18952–18962.
- [24] Z. Su, L. Wang, Y. Li, G. Zhang, H. Zhao, H. Yang, Y. Ma, B. Chu, W. Li, Surface plasmon enhanced organic solar cells with a MoO₃ buffer layer, *ACS Appl. Mater. Interfaces* 5 (2013) 12847–12853.
- [25] Y. Gao, F. Jin, Z. Su, H. Zhao, Y. Luo, B. Chu, W. Li, All thermal-evaporated surface plasmon enhanced organic solar cells by Au nanoparticles, *Org. Electron.* 39 (2016) 71–76.
- [26] F. Jin, B. Chu, W. Li, Z. Su, H. Zhao, C.S. Lee, Enhanced performances in inverted small molecule solar cells by Ag nanoparticles, *Opt. Express* 22 (2014) A1669.
- [27] Y.-M. Sung, Y.-C. Lai, M.-F. Tsai, H.-H. Hsieh, M.-H. Yang, P.P. Wei, C.-S. Yeh, F.-C. Hsu, Y.-F. Chen, Broad band plasmonic nanomaterials for high performance solar cells, *J. Mater. Chem. C* 4 (2016) 513–520.
- [28] Y.-H. Su, Y.-F. Ke, S.-L. Cai, Q.-Y. Yao, Surface plasmon resonance of layer-by-layer gold nanoparticles induced photoelectric current in environmentally-friendly plasmon-sensitized solar cell, *Light Sci. Appl.* 1 (2012) e14.
- [29] S.W. Tong, C.F. Zhang, C.Y. Jiang, G. Liu, Q.D. Ling, E.T. Kang, D.S.H. Chan, C. Zhu, Improvement in the hole collection of polymer solar cells by utilizing gold nanoparticle buffer layer, *Chem. Phys. Lett.* 453 (2008) 73–76.
- [30] M. Xu, J. Feng, Y.-S. Liu, Y. Jin, H.-Y. Wang, H.-B. Sun, Effective and tunable light trapping in bulk heterojunction organic solar cells by employing Au-Ag alloy nanoparticles, *Appl. Phys. Lett.* 105 (2014) 153303.
- [31] L. Lu, Z. Luo, T. Xu, L. Yu, Cooperative plasmonic effect of Ag and Au nanoparticles on enhancing performance of polymer solar cells, *Nano Lett.* 13 (2013) 59–64.
- [32] J. Wang, X. Jia, J. Zhou, L. Pan, S. Huang, X. Chen, Improved performance of polymer solar cells by thermal evaporation of AgAl alloy nanostructures into the hole-transport layer, *ACS Appl. Mater. Interfaces* 8 (2016) 26098–26104.
- [33] W.C. Choy, The emerging multiple metal nanostructures for enhancing the light trapping of thin film organic photovoltaic cells, *Chem. Commun.* 50 (2014) 11984–11993.
- [34] J.-L. Wu, F.-C. Chen, Y.-S. Hsiao, F.-C. Chien, P. Chen, C.-H. Kuo, M.H. Huang, C.-S. Hsu, Surface plasmonic effects of metallic nanoparticles on the performance of polymer bulk heterojunction solar cells, *ACS Nano* 5 (2011) 959–967.
- [35] J.J. Mock, M. Barbic, D.R. Smith, D.A. Schultz, S. Schultz, Shape effects in

- plasmon resonance of individual colloidal silver nanoparticles, *J. Chem. Phys.* 116 (2002) 6755–6759.
- [36] K.-H. Kim, A. Husakou, J. Herrmann, Linear and nonlinear optical characteristics of composites containing metal nanoparticles with different sizes and shapes, *Opt. Express* 18 (2010) 7488–7496.
- [37] X. Li, W.C. Choy, L. Huo, F. Xie, W.E. Sha, B. Ding, X. Guo, Y. Li, J. Hou, J. You, Y. Yang, Dual plasmonic nanostructures for high performance inverted organic solar cells, *Adv. Mater.* 24 (2012) 3046–3052.
- [38] D. Kozanoglu, D.H. Apaydin, A. Cirpan, E.N. Esenturk, Power conversion efficiency enhancement of organic solar cells by addition of gold nanostars, nanorods, and nanospheres, *Org. Electron.* 14 (2013) 1720–1727.
- [39] A.Y. Mahmoud, J. Zhang, D. Ma, R. Izquierdo, V.-V. Truong, Thickness dependent enhanced efficiency of polymer solar cells with gold nanorods embedded in the photoactive layer, *Sol. Energy Mater. Sol. Cells* 116 (2013) 1–8.
- [40] X. Xu, Q. Du, B. Peng, Q. Xiong, L. Hong, H.V. Demir, T.K.S. Wong, A.K. Ko Kyaw, X.W. Sun, Effect of shell thickness on small-molecule solar cells enhanced by dual plasmonic gold-silica nanorods, *Appl. Phys. Lett.* 105 (2014) 113306.
- [41] E. Stratakis, E. Kymakis, Nanoparticle-based plasmonic organic photovoltaic devices, *Mater. Today* 16 (2013) 133–146.
- [42] Q. Xu, F. Liu, Y. Liu, K. Cui, X. Feng, W. Zhang, Y. Huang, Broadband light absorption enhancement in dye-sensitized solar cells with Au-Ag alloy popcorn nanoparticles, *Sci. Rep.* 3 (2013) 2112.
- [43] H.-C. Chen, S.-W. Chou, W.-H. Tseng, I.W.P. Chen, C.-C. Liu, C. Liu, C.-L. Liu, C.-h. Chen, C.-I. Wu, P.-T. Chou, Large AuAg alloy nanoparticles synthesized in organic media using a one-pot reaction: their applications for high-performance bulk heterojunction solar cells, *Adv. Funct. Mater.* 22 (2012) 3975–3984.
- [44] F.-X. Xie, W.C.H. Choy, C.C.D. Wang, W.E.I. Sha, D.D.S. Fung, Improving the efficiency of polymer solar cells by incorporating gold nanoparticles into all polymer layers, *Appl. Phys. Lett.* 99 (2011) 153304.
- [45] C.H. Chou, F.C. Chen, Plasmonic nanostructures for light trapping in organic photovoltaic devices, *Nanoscale* 6 (2014) 8444–8458.
- [46] F.-C. Chen, J.-L. Wu, C.-L. Lee, Y. Hong, C.-H. Kuo, M.H. Huang, Plasmonic-enhanced polymer photovoltaic devices incorporating solution-processable metal nanoparticles, *Appl. Phys. Lett.* 95 (2009) 013305.
- [47] X. Gao, R.J. Esteves, L. Nahar, J. Nowaczyk, I.U. Arachchige, Direct cross-linking of Au/Ag alloy nanoparticles into monolithic aerogels for application in surface-enhanced Raman scattering, *ACS Appl. Mater. Interfaces* 8 (2016) 13076–13085.
- [48] F. Pincella, K. Isozaki, K. Miki, A visible light-driven plasmonic photocatalyst, *Light Sci. Appl.* 3 (2014) e133.
- [49] Y. Xiao, J.P. Yang, P.P. Cheng, J.J. Zhu, Z.Q. Xu, Y.H. Deng, S.T. Lee, Y.Q. Li, J.X. Tang, Surface plasmon-enhanced electroluminescence in organic light-emitting diodes incorporating Au nanoparticles, *Appl. Phys. Lett.* 100 (2012) 013308.
- [50] M. Yao, P. Shen, Y. Liu, B. Chen, W. Guo, S. Ruan, L. Shen, Performance improvement of polymer solar cells by surface-energy-induced dual plasmon resonance, *ACS Appl. Mater. Inter.* 8 (2016) 6183–6189.
- [51] M.C. Ridgway, R. Giulian, D.J. Sprouster, P. Kluth, L.L. Araujo, D.J. Llewellyn, A.P. Byrne, F. Kremer, P.F. Fichtner, G. Rizza, H. Amekura, M. Toulemonde, Role of thermodynamics in the shape transformation of embedded metal nanoparticles induced by swift heavy-ion irradiation, *Phys. Rev. Lett.* 106 (2011) 095505.
- [52] G. Xu, J. Liu, Q. Wang, R. Hui, Z. Chen, V.A. Maroni, J. Wu, Plasmonic graphene transparent conductors, *Adv. Mater.* 24 (2012). OP71–76.
- [53] D. Gaspar, A.C. Pimentel, T. Mateus, J.P. Leitao, J. Soares, B.P. Falcao, A. Araujo, A. Vicente, S.A. Filonovich, H. Aguas, R. Martins, I. Ferreira, Influence of the layer thickness in plasmonic gold nanoparticles produced by thermal evaporation, *Sci. Rep.* 3 (2013) 1469.
- [54] E. Hutter, J.H. Fendler, Exploitation of localized surface plasmon resonance, *Adv. Mater.* 16 (2004) 1685–1706.